Quaternary Science Reviews 125 (2015) 106–116

Contents lists available at ScienceDirect

Quaternary Science Reviews

journal homepage: www.elsevier.com/locate/quascirev

Constraints on southern hemisphere tropical climate change during the Little Ice Age and Younger Dryas based on glacier modeling of the Quelccaya Ice Cap, Peru

Andrew G.O. Malone [a, *], Raymond T. Pierrehumbert [b], Thomas V. Lowell [c], Meredith A. Kelly [d], Justin S. Stroup [d]

[a] Department of the Geophysical Sciences, The University of Chicago, 5734 S. Ellis Ave, Chicago, IL 60637, USA
[b] Department of Physics, Atmospheric Oceanic and Planetary Physics, University of Oxford, OX1 3PU Oxford, United Kingdom
[c] Department of Geology, University of Cincinnati, 500 Geology-Physics Building, Cincinnati, OH 45221, USA
[d] Department of Earth Sciences, Dartmouth College, HB 6105 Fairchild Hall, Hanover, NH 03755, USA

ARTICLE INFO

Article history:
Received 14 March 2015
Received in revised form
29 July 2015
Accepted 1 August 2015
Available online 22 August 2015

Keywords:
Quaternary
Paleoclimatology
Abrupt and centrury-scale climate change events
Tropical glaciers
Glacier modeling

ABSTRACT

Improving the late Quaternary paleoclimate record through climate interpretations of low-latitude glacier length changes advances our understanding of past climate change events and the mechanisms for past, present, and future climate change. Paleotemperature reconstructions at low-latitude glaciers are uniquely fruitful because they can provide both site-specific information and enhanced understanding of regional-scale variations due to the structure of the tropical atmosphere. We produce Little Ice Age (LIA) and Younger Dryas (YD) paleoclimate reconstructions for the Huancané outlet glacier of the Quelccaya Ice Cap (QIC) and low-latitude southern hemisphere regional sea surface temperatures (SSTs) using a coupled ice-flow and energy balance model. We also model the effects of long-term changes in the summit temperature and precipitiation rate and the effects of interannual climate variability on the Huancané glacier length. We find temperature to be the dominant climate driver of glacier length change. Also, we find that interannual climate variability cannot adequately explain glacier advances inferred from the geomorphic record, necessitating that these features were formed during past colder climates. To constrain our LIA reconstruction, we incorporate the QIC ice core record, finding a LIA air temperature cooling at the ice cap of between ~0.7 °C and ~1.1 °C and ~0.4 °C and regional SSTs cooling of ~0.6 °C. For the YD paleoclimate reconstructions, we propose two limits on the precipitation rate, since the ice core record does not extend into the Pleistocene: 1) the precipitation rate scales with the Clausius-Clapeyron relationship (upper limit on cooling) and 2) the precipitation rate increases by 40% (lower limit on cooling), which is an increase about twice as great as the regional increases realized in GCM simulations for the period. The first limit requires ~1.6 °C cooling in ice cap air temperatures and ~0.9 °C cooling in SSTs, and the second limit requires ~1.0 °C cooling in ice cap air temperatures and ~0.5 °C cooling in SSTs. Our temperature reconstructions are in good agreement with the magnitude and trend of GCM simulations that incorporate the forcing mechanisms hypothesized to have caused these climate change events.

1. Introduction

Our understanding of the mechanisms for and the extent of climate change events that occur on sub-Milankovitch cycle timescales is inhibited by under-sampling in the terrestrial low-latitude and southern hemisphere paleoclimate record. Improving this record would increase not only our knowledge about such events but also our understanding of general climate dynamics (Seager and Battisti, 2007). Observed changes in low-latitude and southern hemisphere glacier lengths, since the Last Glacial Maximum (LGM) (26,000–19,500 years ago or 26.5–19.5 ka), can help us improve this record. Changes in glacier length are linked to

* Corresponding author.
E-mail address: amalone@uchicago.edu (A.G.O. Malone).

http://dx.doi.org/10.1016/j.quascirev.2015.08.001

changes in climate, with local meteorology dictating surface mass balance and the local topography and the surface mass balance dictating flow dynamics (Oerlemans and Fortuin, 1992; Oerlemans, 2001). Previous studies have used observations of recent glacier retreats in reconstructions of contemporary climate change (e.g. Oerlemans, 2005; Laclercq and Oerlemans, 2012) and have used geomorphic footprints of past glacier lengths in paleoclimate reconstructions and evaluations (e.g. Rind and Peteet, 1985; Huber et al., 2005; Anderson and Mackintosh, 2006; Doughty et al., 2013).

Paleotemperature reconstructions from tropical mountain glaciers can also provide constraints on past regional temperature change. High-altitude surface temperatures and free atmosphere temperatures deviate only slightly (Seidel and Free, 2003; Bradely et al., 2006), linking temperature changes at tropical glaciers to changes in the free atmosphere. Also, low-latitude horizontal free atmosphere temperature gradients are relatively homogeneous, because the weak Coriolis Force in low-latitudes allows for internal waves to dampen out gradients (i.e. the Weak Temperature Gradient (WTG) approximation) (Pierrehumbert, 1995; Sobel et al., 2001). By the WTG approximation, changes in free atmosphere temperatures at a specific location can be related to broader regional changes at elevation. In addition, low-latitude free atmosphere temperature profiles are dictated by moist convection and the Hadley and Walker circulations, and these dynamical processes link changes in sea surface temperatures (SSTs) to free atmosphere temperature changes according to the moist adiabat curve (Xu and Emanuel, 1989; Pierrehumbert, 1999; Williams et al., 2009). These structures of the tropical atmosphere allow paleotemperature reconstructions for a specific tropical glacier to provide paleotemperature information for other regional glaciers and regional paleo-SSTs.

Before conducting such paleoclimate reconstructions, some outstanding questions must be addressed. First, the climate drivers of tropical glacier length changes are poorly understood. The relative importance of temperature versus precipitation rate changes on tropical glacier length changes is debated (Kaser et al., 2004; Taylor et al., 2006; Thompson et al., 2006; Vuille et al., 2008; Licciardi et al., 2009; Jomelli et al., 2011; Thompson et al., 2013; Stroup et al., 2014; Jomelli et al., 2014). Second, the climate interpretation of glacial geomorphic features is not fully understood. Glacier modeling studies illustrate that glacier length fluctuations can occur due to interannual climate variability within an unchanging mean climate state (Oerlemans, 2000; Roe & O'Neal, 2009; Huybers and Roe, 2009; Roe, 2011; Roe and Baker, 2014). For such a glacier system, the furthest downslope excursion, which is argued to be the location of moraine deposition, may be as much as 15% down-valley from the mean glacier terminus position (Anderson et al., 2014). Such a detachment of the location of the moraine deposit from the mean position of the glacier terminus, which is thought to be determined by the climate, complicates a climate interpretation of the glacial geomorphic record.

We present results from three experiments using a 1-D numerical flow-line model to address these questions and provide paleoclimate constraints for the Little Ice Age (LIA) (~1330–1850 CE) and the Younger Dryas (YD) (~12.8–11.5 ka) for the Huancané outlet glacier of the Quelccaya Ice Cap (QIC), Peru, which is the world's largest tropical ice mass (e.g. Thompson et al., 2006). In Experiment 1, we investigate the glacier length sensitivity of the Huancané glacier to changes in temperature, precipitation rate, and summit accumulation rate. In Experiment 2, we determine temperature and precipitation rate changes that can produce the LIA and YD glacier lengths. For the LIA glacier length we incorporate the QIC ice core record (Thompson et al., 1985, 1986, 2013) to constrain better our reconstructions. In Experiment 3, we investigate the glacier length response to interannual climate variability.

1.1. Study site

The QIC, located in the Cordillera Oriental of the Andes [13.9 °S, 70.9 °W; 55 km^2; summit altitude 5670 m.a.s.l; Fig. 1], sits atop an ignimbrite plateau (Audebaud, 1973; Chavez et al., 1997) with multiple valleys connecting the plateau to the surrounding landscape that contain glacial features (Mercer et al., 1975; Mercer and Palacios, 1977; Goodman et al., 2001; Mark et al., 2002; Kelly et al., 2012; Stroup et al., 2014; Kelly et al., 2015). The Rio Huancané valley, on the southwest side of the QIC (Fig. 1), contains three prominent moraine belts: 1) Huancané I (Hu-I) (~1 km downslope from the current ice margin), 2) Huancané II (Hu-II) (~4 km downslope), and 3) Huancané III (Hu-III) (~8 km downslope) (Mercer et al., 1975; Mercer and Palacios, 1977). The Hu-I moraines date to the LIA (Mercer and Palacios, 1977; Stroup et al., 2014) and may mark the maximum Holocene glacier extent (Stroup et al., 2014). The Hu-II moraines mark a readvance of the glacier at the end of the Lateglacial Period (Mercer and Palacios, 1977; Goodman et al., 2001; Kelly et al., 2012, 2015) and have been constrained to 12.35 + 0.2, −0.02 ka, indicating an ice advance during the early to middle YD (Kelly et al., 2012, 2015). The Hu-III moraines are attributed to the LGM or a standstill in the early part of the retreat from the LGM (Mercer and Palacios, 1977; Goodman et al., 2001; Kelly et al., 2015) and are not studied in this paper.

2. Glacier model & experiments

In this work, we use a shallow-ice 1-D glacier flowline model coupled to an energy balance ablation model. Similar methods have been used (though the ablation schemes have varied) to explore glacier length sensitivity to different types of climate change, make predictions about future glacier length changes, study glacier response to interannual climate variability, and reconstruct paleoclimates associated with glacial geomorphic features (e.g. Oerlemans, 1986; Oerlemans, 1997a,b, 2000; Anderson and Mackintosh, 2006; Roe & O'Neal, 2009).

2.1. Glacier flow model

We use a shallow-ice 1-D glacier flowline model to simulate the ice flow, which has been shown to capture mountain glacier flow dynamics (Oerlemans, 1986). The governing equation is the 1-D mass continuity equation for a constant density fluid:

$$\frac{\partial}{\partial t}(H) = -\frac{1}{w}\frac{\partial}{\partial x}(u\,H\,w) + B$$

where H is the ice thickness, t is time, w is the valley width, x is the position along the flowline, u is the sum of the vertically averaged deformation velocity (u_d) and sliding velocity (u_s) in the direction of the flowline, and B is the surface mass balance (see Section 2.2). We use a trapezoidal approximation for w (see Oerlemans, 1997a). Velocity relationships follow Oerlemans (1997a, 2000):

$$u_d = f_d H \tau^3$$

and

$$u_s = f_s H^{-1} \tau^3$$

where τ is the local driving stress ($-\rho\, g\, H \frac{\partial h}{\partial x}$), g is the acceleration of gravity, ρ is the ice density (910 kg m^{-3}), H is the ice thickness, $\frac{\partial h}{\partial x}$ is

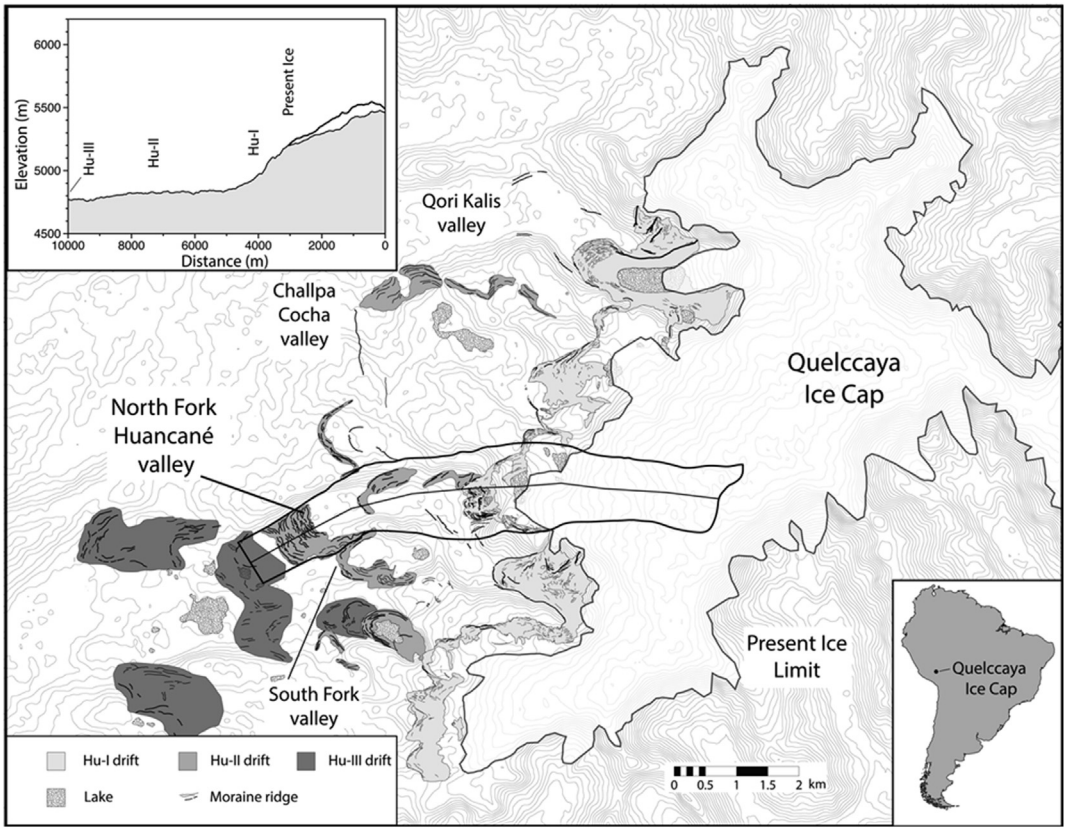

Fig. 1. Glacier geologic map of the three outlet glaciers on the west side of the Quelccaya Ice Cap (south-eastern Peru) (Adapted from Kelly et al., 2012). The outlined area indicates the North Fork of the Rio Huancané Valley (focus area). The flowline along the valley is indicated by the line in the middle of the outline. The insert on the top left is the characteristic bedrock profile of the valley.

the slope of the glacier surface, f_d is the deformation parameter, and f_s is the sliding parameter. For f_d we use 1.9×10^{-24} Pa^{-3} s^{-1}, and for f_s we use 5.7×10^{-20} Pa^{-3} m^2 s^{-1} (Oerlemans, 1997a).

We use data from the Shuttle Rader Topography Mission (http://srtm.usgs.gov/index.php) to construct the flowline geometry of the Huancané valley, with a spatial resolution of 50 m and a model domain that extends 250 m beyond the characteristic position of the Hu-II moraines. We solve the flow dynamics using the Crank-Nicholson method and a time-step of one model month.

2.2. Surface energy mass balance model

We calculate the surface mass balance, B, from the difference between the solid precipitation and the ablation at each position, x, along the flowline. The ablation rate is calculated from an energy balance model. The available melt energy, Q_m, when the ice surface is at the melting temperature, is calculated from the following equation:

$$Q_m = S + L + Q_H + Q_E + Q_R$$

where S is the net shortwave radiation absorbed by the ice, L is the net longwave radiation, Q_H is the sensible heat flux, Q_E is the latent heat flux, and Q_R is the heat flux due to rain on the ice surface. Refreezing of melt water is not included in this model, and all meltwater is assumed to be lost from the system by either runoff or evaporation. S and L follow the parameterizations outlined in Pierrehumbert (2011). Q_H and Q_E follow the bulk method with the Richardson stability criterion for stable stratification (Hock, 2005). We also calculate the amount of mass loss from sublimation when Q_E is negative (energy flux out of the ice) but do not include mass deposition when Q_E is positive (energy flux into the ice).

We use monthly mean data from a meteorological station on the QIC summit from August 2004 to June 2012 managed by the University of Massachusetts (correspondence with Dr. Doug Hardy) to constrain the energy balance model parameters and contemporary summit temperature signal. We use monthly mean data from the Tropical Rainfall Measuring Mission (TRMM) (Bookhagen and Strecker, 2008) for the contemporary precipitation rate signal, which captures the seasonality in the QIC precipitation rate. The TRMM data produces a smaller net annual precipitation rate than the Thompson et al. (2013) observed summit accumulation rate, and we scale up the TRMM precipitation signal to a net annual precipitation rate of 1.34 m w.e. a^{-1}, while not changing the seasonality of the precipitation rate. With this scaling, the model produces the Thompson et al. (2013) contemporary QIC summit accumulation rate while producing the modern terminus position. We assume that the valley air temperature follows a linear temperature profile with a lapse rate of 5.4 °C km^{-1}, which is the value for the QIC from Bradley et al. (2009). We also conduct experiments with a temperature dependent lapse rate (see Section 2.3).

2.3. Equilibrium glacier length simulations (Experiments 1 & 2)

In Experiments 1 and 2, we calculate the equilibrium glacier length and accumulation rate along the flowline for a given temperature and precipitation pairing. We start the model with a zero-height profile and run it until it reaches an equilibrium height

profile. To perturb the climate, we vary the mean summit temperature from −2.50 °C to +1.15 °C around the contemporary value in increments of 0.05 °C and the precipitation rate from −90% to +225% times the contemporary value in increments of 5%. In Experiment 1, we fix either the temperature or precipitation rate at the contemporary signal and vary the other climate forcing, running the model to equilibrium each time. In Experiment 2, we run the model to equilibrium with each pairing of temperature and precipitation rate changes (n = 4864) and find the combinations of perturbations that can produce an equilibrium glacier length that reaches the characteristic position of the Hu-I or Hu-II moraines along the flowline. For the Hu-I moraines (LIA-aged), we incorporate the decadal-average summit accumulation record (Thompson et al., 2013) to find the combinations of temperature and precipitation rate change that can both advance the glacier to the Hu-I position and produce the summit accumulation rate appropriate for the time of moraine deposition. We reconstruct temperature and precipitation rate changes for the Hu-I and Hu-II features since they are within the same valley basin, but we cannot reconstruct the Hu-III features because the ice likely extended above the valley basin that contained the glacier during the time of deposition of the Hu-I and Hu-II moraines, requiring methods beyond the scope of this paper.

In Experiment 2, we use the method from Pierrehumbert (1999) to relate our calculated temperature changes at the ice cap to regional SST changes by extrapolating along the saturated moist adiabat temperature profile to sea level. For this method to be appropriate, both the WTG approximation and the assumption that the free atmospheric temperature profile follows the moist adiabat curve must hold. We validate the WTG approximation by calculating the 500 mbar free atmosphere temperature at the QIC latitude using NCEP/NCAR Reanalysis 1 output (http://www.esrl.noaa.gov/psd), finding for a longitudinal sweep that it varies by less than ±1 °C around the mean, which is consistent with the WTG approximation (Pierrehumbert, 1995). We validate the second assumption by calculating the locally linear lapse rate at the QIC summit elevation of the moist adiabat curve that produces the observed summit temperature at the elevation of the meteorology station, finding it to be ~5.4 °C km^{-1}, which agrees with the previously published value (Bradley et al., 2009). Although the moist adiabat curve is nonlinear, it is linear to first order over the elevation range of the QIC, allowing us to use a constant lapse rate for the surface energy balance ablation model. However, over greater elevation ranges, this non-linear structure is important. The locally linear lapse rate of the moist adiabat curve steepens with height making temperature changes in the free atmosphere at the elevation of Peruvian Andes glaciers amplified relative to the corresponding SST changes.

In both Experiments 1 and 2 we use two different lapse rate schemes. For the first scheme, we hold the lapse rate fixed at the contemporary value (5.4 °C km^{-1}). For the second scheme, we allow the lapse rate to vary with changes in the mean temperature. Since the temperature profile follows the moist adiabat curve, which has a curvature that is dependent on regional temperatures, the locally linear slope of moist adiabat curve (i.e. the lapse rate) at the elevation of the QIC varies with regional temperature changes. As regional temperatures increase, the lapse rate at the QIC decreases, and as regional temperatures decrease it increases. See Table 1 for the summit temperature changes, SST changes, and lapse rates characteristic of the experiments.

2.4. Interannual climate variability simulations (Experiment 3)

In Experiment 3, we add interannual temperature and precipitation rate variability to the climate signal while not changing the mean state. We run the model to equilibrium without climate variability and then add a stochastic noise term to both the temperature and precipitation rate signals, running it for an additional 11,000 model years. The stochastic noise term is produced by a Gaussian random number generator with a prescribed standard deviation (1−σ value). These climate perturbations are uncorrelated from one model-year to the next but persist for the entire model year. The time duration of these perturbations affects the magnitude of the glacier response, with a one time-step duration (one model-month) perturbation producing a lesser magnitude of glacier response than a perturbation that persists for an entire model year for a fixed noise variance. For consistency with previous studies (e.g. Roe and O'Neal, 2009; Huybers and Roe, 2009; Roe, 2011; Anderson et al., 2014; Roe and Baker, 2014), we use a correlation time of one model-year. Also for consistency, the temperature and precipitation rate anomalies are uncorrelated with each other. For the temperature variance, we perturb the annual mean but not the seasonal cycle, and for the precipitation rate variance, we perturb the net precipitation but not the seasonal cycle. We run simulations with a 1−σ value of the annual-averaged summit temperature time series ranging from 0.0 °C to 0.75 °C, in intervals of 0.05 °C and a 1−σ value of the net annual precipitation time series ranging from 0% to 50% the current amount, in intervals of 5%. We conduct a simulation for every combination of temperature and precipitation rate variance (n = 176). For statistics, we discard the first 1000 years of output, using only the last 10,000 years.

Table 1
Temperature changes and lapse rate for simulations.

ΔT_{summit} (°C)	ΔSST (°C)	Lapse rate (°C km^{-1})
−2.50	−1.35	5.72
−2.00	−1.09	5.65
−1.50	−0.82	5.59
−1.00	−0.55	5.52
−0.50	−0.27	5.46
0.00	**0.00**	**5.40**
+0.50	0.28	5.34
+1.00	0.55	5.28
+1.50	0.83	5.22

Bold values in this table correspond to no temperature change, i.e. essentially the 'control'.

3. Results

3.1. Experiment 1: climate drivers of glacier length change

The glacier responds differently to summit air temperature changes than to precipitation rate changes (Fig. 2a). The rate of glacier length change due to an air temperature change varies across the valley, depending on the valley slope and to a lesser degree the lapse rate scheme. In contrast, the rate of length change due to precipitation rate changes is constant for most of the valley. The slope of the Huancané valley steepens along the flowline from the top of the ice cap to the base of the plateau (~4700 m along the flowline) at which point the slope becomes negligible (<1°) (see insert in Fig. 1). Along the steepest section (from roughly the current ice margin past the Hu-I moraines to the base of the plateau), the length change due to an air temperature change is the smallest, with a rate of ~1000 m per °C for the contemporary lapse rate scheme and a rate of ~900 m per °C for the temperature dependent lapse rate scheme. Upslope from the ice margin to ~2000 m along the flowline the valley slope is shallower, and the rate of length change increases, with a rate of ~1750 m per ° C (contemporary lapse rate) or ~1700 m per °C (temperature dependent lapse rate). The topmost ~2000 m of the valley is the shallowest (until the plateau base), and the rate of length change is even larger, with a

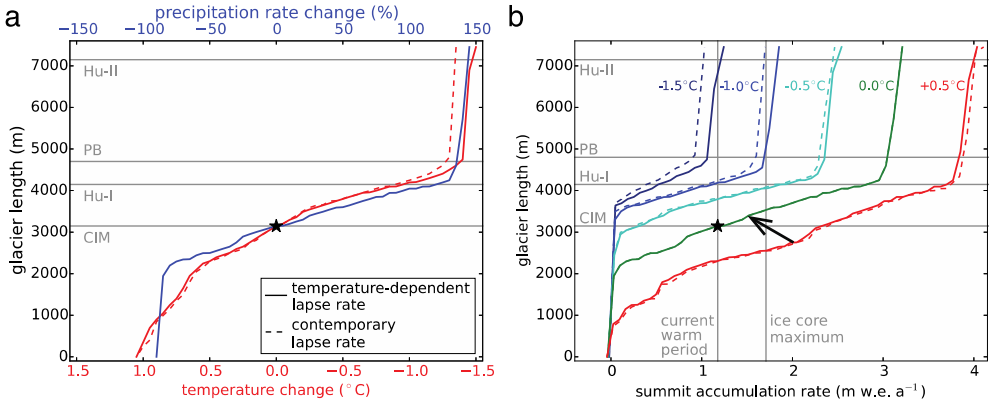

Fig. 2. Climate drivers of Huancané glacier length changes. a) Glacier length sensitivity to precipitation rate changes and air temperature. Notice the differences in scale of the x-axes. b) Glacier length sensitivity to summit accumulation rate changes along different summit isotherms ranging from −1.5 °C (dark blue curve) to +0.5 °C (red curve). The black arrow indicates a ~650 m glacier advance from a 0.5 m w.e. a^{-1} reduction in the summit accumulation rate and a 0.5 °C cooling. The current accumulation rate and maximum decadal-average accumulation rate from the QIC ice core (Thompson et al., 2013) are plotted. In both figures, the current climatology is indicated by the black star, and the location of the current ice margin (CIM), Hu-I moraines (Hu-I), plateau base (PB), and Hu-II moraines (Hu-II) are indicated. (For interpretation of the references to color in this figure caption, the reader is referred to the web version of this article.)

rate of ~4200 m per °C (contemporary lapse rate) and ~4250 m per °C (temperature dependent lapse rate). The length change due to precipitation rate changes is constant from the point of deglaciation to the base of the plateau, with a rate of ~1000 m per doubling. When the terminus reaches the base of the plateau, slight changes in either temperature or precipitiation rate result in large length changes.

The summit accumulation rate record also provides information about glacier length change but must be interpreted with knowledge of ice cap air temperatures (Fig. 2b). For a fixed summit air temperature, the glacier will advance with increased summit accumulation and retreat with decreased summit accumulation. However, significant glacier length advances can also occur at a fixed or decreased summit accumulation rate due to air temperature cooling at the ice cap (black arrow in Fig. 2b). For most of the valley, air temperature changes produce greater length changes than those produced by accumulation rate changes, but once the terminus reaches the plateau base, the glacier becomes highly sensitive to any climate change.

To compare the importance of each climate forcing, we determine the change required to advance the glacier to the nearest moraine location when only varying one climate forcing. An advance to the Hu-I moraine location, in the absence of an air temperature change, requires a precipitation rate increase of 120% (1.60 m w.e. a^{-1} increase) or summit accumulation rate increase of 140% (1.64 m w.e a^{-1} increase). The largest observed increase in the decadal-average accumulation rate from the QIC ice core record is ~45% (0.53 m w.e. a^{-1} relative to the Current Warm Period) (Thompson et al., 2013), which in the absence of cooling would only produce a ~400 m length advance if sustained long enough for the glacier to reach a new equilibrium position. In contrast, an advance to the Hu-I moraines due to only air temperature change requires a cooling of 0.90 °C (contemporary lapse rate) or 0.95 °C (temperature-dependent lapse rate). Experiment 1 highlights the strong relationship between temperature changes and glacier length changes and the weaker relationships between glacier length change and precipitation rate or summit accumulation rate changes. It also highlights the importance of cooling in the formation of the observed glacial features in the Huancané valley.

3.2. Experiment 2: possible LIA & YD paleoclimates

We find combinations of temperature and precipitation rate changes that can produce an equilibrium glacier length at the position of the Hu-I moraines (LIA-age) or the Hu-II moraines (YD-age) (Fig. 3). We further constrain LIA changes by using the QIC ice core record (Thompson et al., 2013) and by assuming that the Huancané valley LIA glacial chronology matches the chronology for the QIC's Qori Kalis valley. In the Qori Kalis valley, the glacier retreated from its maximum LIA extent ~1490 CE ± 60 years and readvanced to a lesser extent between 1660 CE and 1710 CE (Stroup et al., 2014). The climate forcing associated with this earlier moraine age must have predated the reconstructed age, placing the climate forcing during a period of decreased summit accumulation (~13% decrease). The age of the readvance is concurrent with the tail end of a period of increased summit accumulation (~27% increase) (Thompson et al., 2013), and the climate forcing associated with the readvance most likely included increased accumulation.

For the earlier LIA moraine age (~1490 CE +/60), an air

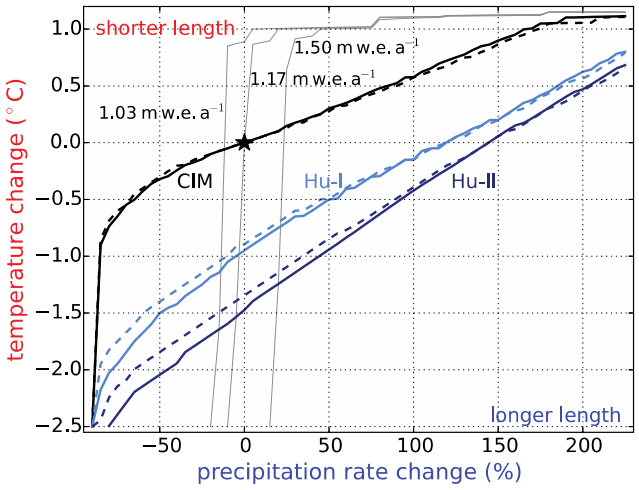

Fig. 3. Air temperature and precipitation rate changes that can produce a glacier length at the current ice margin (CIM), Hu-I moraines (Hu-I), or Hu-II moraines (Hu-II) for the contemporary lapse rate (dashed curves) and the temperature-dependent lapse rate (solid curves). The summit accumulation rate is calculated for each temperature and precipitation rate change, and the thin gray curves indicate the accumulation rate for the current period (1.17 m w.e. a^{-1}), the earlier LIA period (1.03 m w.e. a^{-1}), and the later LIA period (1.50 m w.e. a^{-1}) (Thompson et al., 2013). The black star indicates the current climatology.

temperature cooling 1.03 °C for the contemporary lapse rate scheme or 1.13 °C for the temperature-dependent lapse rate scheme and a precipitation decrease of ~14% (0.19 m w.e. a^{-1}) produce an equilibrium glacier length at the Hu-I moraine position and the summit accumulation rate for the period just before the earlier age (1.026 m w.e. a^{-1}). For the later LIA moraine age (1660 CE and 1710 CE), a cooling of 0.69 °C (contemporary lapse rate) or 0.74 °C (temperature-dependent lapse rate) and precipitation rate increase of ~21% (0.28 m w.e. a^{-1}) produce an equilibrium length at the Hu-I moraines the summit accumulation rate for the period before the later age (1.504 m w.e. a^{-1}). Extrapolating these summit air temperature coolings along the moist adiabat curve to sea level, we find an SST cooling of between 0.56 °C and 0.62 °C for the earlier period and between 0.38 °C and 0.41 °C for the later period.

The QIC ice core record does not extend into the late Pleistocene, but we constrain the possible changes for the Hu-II moraines (YD-age) by exploring two types of precipitation rate change. In the first type, we assume that there is not a change in regional circulation, and the precipitation rate scales with Clausius–Clapeyron, where a 1 °C cooling results in a ~7% decrease in the precipitation rate. In the second type, we assume that there are changes in the regional circulation pattern that increase QIC precipitation. GCM simulations suggest that increased northern hemisphere sea ice during the YD forced the intertropical convergence zone (ITCZ) southward (Chiang and Bitz, 2005), providing a mechanism for increased precipitation in the southern tropical Andes. Dynamic GCM simulations of the last 22,000 years show increased precipitation for the gridcells near the QIC during the YD (Liu et al., 2009; He, 2011; He et al., 2013). Also, geological evidence supports increased late-Pleistocene precipitation for the southern tropical Andes, with higher lake levels at Lake Titicaca (Baker et al., 2001), large paleolakes in southern Bolivia (Placzek et al., 2006), and increased net accumulation at nearby glacier Sajama (Bolivia) (Thompson et al., 1998).

For the first type of precipitation rate change (Clausius–Clapeyron scaling), a greater cooling is required than for the second type (increased precipitation rate). For the first type, a cooling of 1.45 °C (contemporary lapse rate) or 1.59 °C (temperature-dependent lapse rate), corresponding to a precipitation rate decrease of ~10% (0.14 m w.e. a^{-1}), produces an equilibrium glacier length at the Hu-II moraines. These summit air temperature coolings correspond to SST coolings of between 0.79 °C and 0.87 °C. For the second type, a 20% increase in the precipitation rate, which is consistent with GCM output (Liu et al., 2009; He, 2011; He et al., 2013), and summit cooling of 1.14 °C (contemporary lapse rate) or 1.24 °C (temperature-dependent lapse rate) produce an equilibrium glacier length at the Hu-II moraines. These summit air temperature coolings correspond to SST coolings of between 0.63 °C and 0.68 °C. For an upper extreme on the YD precipitation rate increases (and lower extreme on YD cooling), we increase the precipitation rate by 40%, and a cooling of 0.94 °C (contemporary lapse rate simulations) or 1.04 °C (temperature-dependent lapse rate simulations) produces an equilibrium glacier length at the position of the Hu-II moraines. These summit air temperature coolings correspond to SST coolings of between 0.52 °C and 0.57 °C.

3.3. Experiment 3: glacier length response to interannual annual climate variability

We quantify the expected glacier length fluctuations from contemporary climate variability at the QIC using the CRU TS v3.22 monthly mean observational data set (Harris et al., 2014), finding a 1−σ value of the detrended annual mean temperature time series of 0.52 °C and of the precipitation rate time series of 15% (Fig. 4a). The two anomaly signals are uncorrelated (r = −0.10), consistent

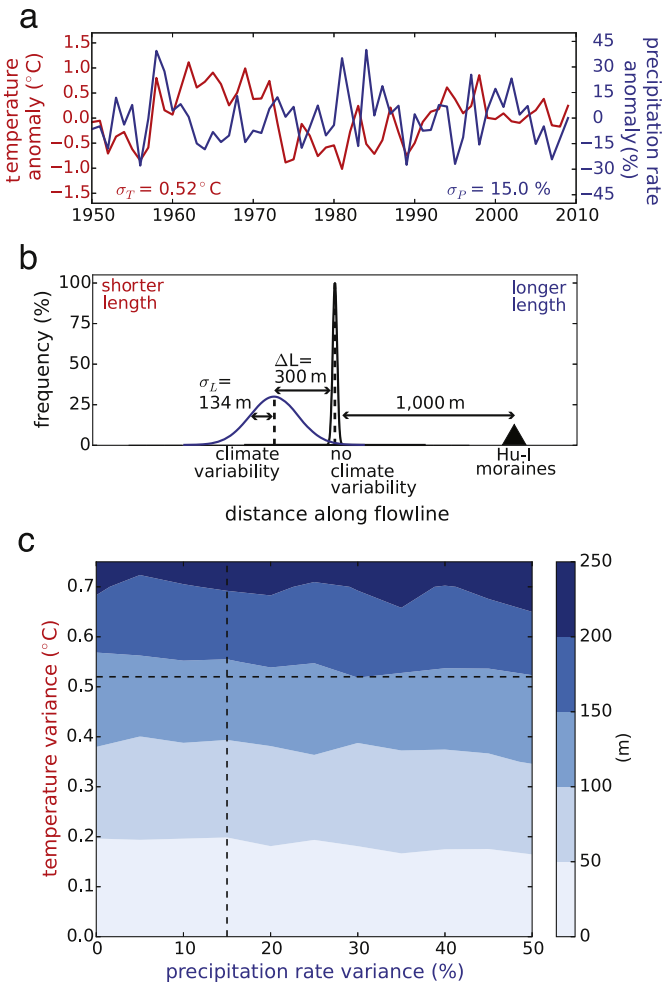

Fig. 4. Climate variability and glacier response to climate variability. a) QIC detrended annual mean anomalies in temperature and precipitation rate from the CRU TS v3.22 monthly mean observational data set (01/1950–12/2009) (Harris et al., 2014). The temperature and precipitation rate variances (1−σ values) are included, and the correlation coefficient between the time series is r = −0.10. b) Huancané glacier response to observed climate variability. Without climate variability, the terminus remains at a constant position (black delta function), but with climate variability the terminus fluctuates around the mean position (blue normal distribution), with the included 1−σ value (σ_L). Also, climate variability causes an upslope retreat (ΔL) compared to the equilibrium position without climate variability. c) Magnitude of glacier length fluctuations due to a range of climate variability values. The magnitude (in meters) is the 1−σ value of the glacier length time series. The observed precipitation rate (vertical dashed line) and temperature (horizontal dashed line) variances are included. The magnitude of fluctuations depends on the temperature variance but is mostly independent of the precipitation rate variance. (For interpretation of the references to color in this figure caption, the reader is referred to the web version of this article.)

with our methodology. For these climate variances, the 1−σ value of the glacier length time series (magnitude of glacier length fluctuations) is 134 m (Fig. 4b). However, with such climate variance, the mean terminus position also retreats 300 m upslope from the terminus position of the glacier in simulations without climate variability (Fig. 4b). Assuming that the 3−σ value of the glacier length time series is the maximum excursion that could produce an observable feature, features within ~400 m of the terminus may be accounted for by glacier fluctuations due to climate noise, which is far less than the advance necessary to produce the closest moraines. However, the mean glacier terminus position also retreats 300 m upslope, reducing any downslope excursions of the glacier beyond the equilibrium terminus position in simulations without

climate variability.

The Huancané glacier also responds differently to noise in the temperature signal (temperature variances) than to noise in the precipitation rate signal (precipitation variance). The magnitude of glacier length fluctuations increases with greater temperature variance but is mostly invariant to the amount of precipitation rate variance (Fig. 4c). The maximum 1−σ value of glacier length fluctuations is 244 m, and occurs when the temperature variance is greatest (1−σ value of the temperature anomaly time series is 0.75 °C). When the temperature variance is <0.2 °C, the 1−σ value of the glacier length fluctuations is less than 50 m (i.e. smaller than the model spatial resolution). Also, the amount of retreat in the mean terminus position (compared to simulations without climate noise) depends on the amount of temperature variance, but it is mostly insensitive to the amount of precipitation rate variance (not shown). The glacier length retreat increases with greater temperature variance, and the maximum retreat is ~700 m when the temperature variance is 0.75 °C. Experiment 3 highlights different responses of the glacier to temperature and precipitation rate variance and also illustrates that downslope excursions of the glacier due to interannual climate variability cannot produce the glacial features in the Huancané valley.

4. Discussion

We find that air temperature changes are the major climate driver of length changes of the Huancané glacier. The glacier advance for a 1 °C cooling is between one and four times the amount of advance for a doubling in the precipitation rate. Air temperature changes have been shown to be the dominant mechanism for length changes for mid and high latitude glaciers (Anderson and Mackintosh, 2006), and we suggest that this is also the case for low-latitude glaciers. Sagredo et al. (2014) show that tropical glaciers have a greater sensitivity in their equilibrium line altitudes (ELA) to air temperature changes than to precipitation rate changes and that many low-latitude glaciers have larger temperature sensitivity than mid and high latitude glaciers. Further, Sagredo et al. (2014) find that low-latitude glaciers require precipitation rate increases of between ~100% and ~300% to balance the ELA change from a 1 °C warming, while mid-latitude South American glaciers require a precipitiation rate increase of ~33%. For mid and high latitude glaciers, values of ~25% have been more broadly used (Braithwaite and Zhang, 2000; Oerlemans, 2001). We find that the Huancané glacier requires a precipitation rate increase of ~170% to offset the retreat for a 1 °C warming.

Climatology may account for why changes in tropical glacier lengths are dominated by air temperature changes. Mild temperature seasonality in the tropics creates a relatively constant snowline (Kaser, 1995), limiting solid accumulation to the upper parts of tropical glaciers and restricting the size of the accumulation area. In addition, 70–80% of the QIC precipitation falls during the austral summer (Thompson et al., 2013), when the snowline is the highest, and glaciers with maximum summer precipitation are especially sensitive to temperature changes (Fujita, 2008a, 2008b). Further, the shallow low-latitude lapse rate causes greater vertical displacement in the freezing line for a given temperature change than for glaciers with a steeper lapse rate which, coupled with the low temperature seasonality in the tropics, amplifies ELA changes. In addition, recent work finds amplified warming in high-altitude mountain regions (where all tropical glaciers are found) due to mechanisms both included and not included in this study, which may further increase the sensitivity of tropical glaciers to regional air temperature changes (Pepin et al., 2015). The especially high sensitivity of the Huancané glacier length to air temperature changes may also be due to the hypsometry of the QIC (see insert in Fig. 1). The accumulation area is a flat plateau, making the ice cap especially vulnerable to shifts in the freezing height (Mark et al., 2002). However, the large response of the Huancané glacier length to air temperature changes should also be realized at other low-latitude glaciers due to the constraints placed by climatology.

We find that the observable glacial features in the Huancané valley could only have been formed during past cooler climates. To reproduce the Hu-I or Hu-II moraines in the absence of regional cooling requires a more than doubling in the precipitation rate, which exceeds any long-term anomalies in the ice core accumulation record (Thompson et al., 2013) or regional precipitiation rate increases realized in GCM simulations of the late Pleistocene and Holocene (González-Rouco et al., 2006; Liu et al., 2009; He, 2011; He et al., 2013) (see Fig. 5b and Fig. 6b). However, significant glacier advances can occur during periods of unchanged or even decreased summit accumulation due to air temperature coolings at the glacier (Fig. 2b). Our modeling results are consistent with interpretations from Stroup et al. (2014), which suggest that regional cooling during a period of decreased summit accumulation provided the climate forcing for the maximum late Holocene glacial extent of the QIC's Qori Kalis glacier. Finally, we find that the magnitude of glacier length fluctuations due to contemporary interannual climate variability is far less than the advances necessary to form the glacial features in the Huancané valley. Glacier features within ~400 m of the terminus position could be formed due to contemporary interannual climate variability but the closest downslope moraines require an advance of ~1000 m.

The response of the Huancané glacier to interannual climate variability differs from previous studies of mid-latitude glaciers (e.g. Oerlemans, 2000; Roe & O'Neal, 2009; Huybers and Roe, 2009; Roe, 2011; Anderson et al., 2014; Roe and Baker, 2014). We find that the magnitude of Huancané glacier length fluctuations depends mainly on the amount of temperature variability and is insensitive to precipitiation rate variability (Fig. 4c), unlike for mid-latitude

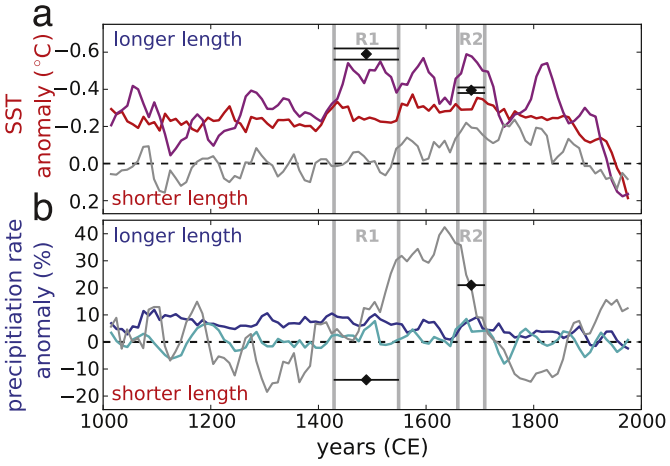

Fig. 5. Little Ice Age (LIA) paleoclimate reconstructions of a) SST anomalies from the TraCE GCM simulation (Liu et al., 2009; He, 2011; He et al., 2013) (red curve), the González-Rouco et al. (2006) GCM simulation (magenta curve), reconstructions of the NINO4 region from the Thompson et al. (2013) $\delta^{18}O$ ice core record (gray curve), and this study (black diamonds with error bars) and b) precipitation rate anomalies from TraCE simulation and González-Rouco et al. (2006) simulation (cyan), accumulation rate anomaly from the Thompson et al. (2013) ice core record (gray curve), and this study (black diamonds with error bars). R1 indicates the age-range of the earlier LIA period, and R2 indicates the age-range of the latter LIA period. SST anomalies from GCM output are for the region 1.8°S to 20.4°S; 108.7°W to 18.7°W. Precipitation rate anomalies from GCM output are for the grid cells adjacent to the QIC. All curves are decadal-averaged anomalies relative to the 1900–1990 CE mean and smoothed with a 30-year running mean. (For interpretation of the references to color in this figure caption, the reader is referred to the web version of this article.)

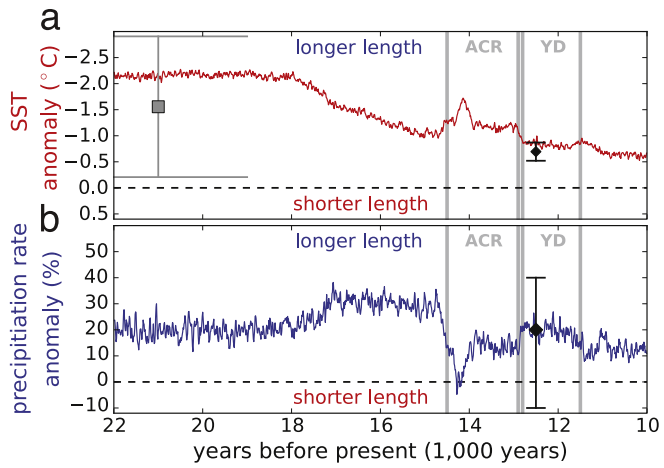

Fig. 6. Younger Dryas (YD) paleoclimate reconstructions of a) SST anomalies from the TraCE GCM simulation (red curve), the MARGO SST reconstructions (Waelbroeck et al., 2009) for the same region as the GCM (gray square with error bars), and this study (black diamond with error bars) and b) precipitation rate anomalies from the TraCE simulation and this study (black diamond with error bars). The Antarctic Cold Reversal (ACR) and YD are indicated. The geographic regions and averaging and soothing are the same as for Fig. 5. (For interpretation of the references to color in this figure caption, the reader is referred to the web version of this article.)

glaciers, where both temperature and precipitation play a role. This strong dependence on temperature and minimal dependence on precipitation rate mirrors the trend for length sensitivity (Section 3.1) and is likely also due to climatology. Mass surpluses (or deficits) from precipitation rate anomalies are confined to the upper regions of the glacier and must be transported to the toe of the glacier before causing length variations. The glacier transport time is greater than the correlation time of the climate variability (one model year), and these imbalances are likely offset before reaching the terminus. By comparison, temperature variability affects both the melt rate on the lower parts of the glacier and the elevation of the freezing line, resulting in shorter response times to temperature anomalies than to precipitation rate anomalies. An additional result from simulations with climate noise is that the mean glacier length retreats (compared to the terminus position in simulations without noise) with increased temperature noise, suggesting that a glacier will retreat more from a few warm years than advance from a few cold ones. Some of this asymmetry between advance and retreat may also reflect variations in the slope of the valley bedrock (see insert in Fig. 1). This upslope retreat of the mean terminus position with increased temperature variance also suggests that a glacier's equilibrium terminus position may be dependent on more than just the mean state (mean annual temperature and net annual precipitation). Fujita (2008a,b), Vacco et al. (2009) and Sagredo et al. (2014) have shown that seasonality plays an important role in the glacier mass balance, length, and ELA, and our results suggest that climate variability can also play a role in determining the mean terminus position.

We reconstruct ice cap air temperature decreases relative to the present for the LIA and YD, finding a cooling of between 0.69 °C and 1.13 °C for the LIA and between 0.94 °C and 1.59 °C for the YD. The colder YD climates inferred from this study as well as GCM results (Liu et al., 2009; He, 2011; He et al., 2013) and isotope anomaly measurements at other tropical Andean ice masses (Thompson et al., 1995, 1998; Ramirez et al., 2003) may have caused a different basal thermal regime, which would have affected the glacier flow dynamics. Ice core temperature profiles indicate that the modern base of the glacier is at the pressure melting point, allowing for basal sliding, even though interior parts of the ice core are below the pressure melting point (Thompson et al., 2013). Also, many boulders emerging from the current ice margin are striated, indicating recent basal sliding (Kelly et al., 2015). However, middle Holocene-age in situ organic matter exposed from beneath the currently retreating ice margin (e.g. Thompson et al., 2013) suggests that basal sliding may be limited in places today, and given the non-temperate glacier characteristics from the ice core and the in situ organic matter, basal freezing may be been more prevalent in past colder climates, limiting basal sliding. Our flowline model includes deformation and basal sliding velocities and parameterizations calibrated for both transport modes (Oerlemans, 1986, 1997a,b). While exploring the effects of each type of motion on the paleoclimate reconstructions is beyond the scope of this study, our work can place absolute constraints on air temperature coolings from limits on changes in freezing level height inferred from the hypsometry of Quelccaya Ice Cap (see the insert in Fig. 1). This limit is independent of the types of ice transport. The freezing level cannot be displaced more than ~500 m due to air temperature cooling before solid accumulation would fall on most of the valley and ablation would be suppressed to the point where almost limitless glacier growth could occur. Such conditions are not observed during the time of the Hu-II moraines deposition. Our modeled zero degree isotherm is ~5000 m.a.s.l and the mean position of the zero degree isotherm during the austral summer months is ~5300 m.a.s.l, which we use as an estimate of the snowline due to the climatology at the QIC. These values agree well with previous estimates (Mercer and Palacios, 1977; Thompson, 1979). To displace the snowline from the current position to the base of the plateau requires a cooling of ~2.4 °C (contemporary lapse rate) or ~2.6 °C (temperature-dependent lapse rate), which corresponds to SST coolings of 1.3 °C and 1.4 °C. These coolings are an extreme upper limit, and runaway glacier growth would likely occur at even lesser amounts of cooling, due to feedbacks between the height of the ice surface and the rate of ablation. Even for this upper limit on cooling, YD ice cap air temperatures would only be ~1 °C to ~1.4 °C colder than the values determined from the flowline model, and SSTs would only be ~0.5 °C–~0.8 °C colder.

We reconstruct regional SST changes for two periods during the LIA based on the chronology at the Qori Kalis valley of the QIC. These two periods are concurrent with Northern Hemisphere temperature depressions (Mann et al., 2009) and late Holocene glacier fluctuations in the tropical Andes and in the Northern Hemisphere (Licciardi et al., 2009; Jomelli et al., 2009). For the earlier period (1490 CE ± 60 years), we find a precipitation rate decrease of ~14% and a regional SST cooling of between 0.56 °C and 0.62 °C. For the latter period (1660–1710 CE), we find a precipitation rate increase of ~21% and a regional SST cooling of between 0.38 °C and 0.41 °C. The González-Rouco et al. (2006) GCM simulation (GR) of the last millennium, forced with greenhouse gas reconstructions from ice cores, short-term solar variations, and volcanic aerosols, finds a cooling during these periods in the global and northern hemisphere surface temperatures and the southern hemisphere tropical SSTs (Fig. 5a). During the early period, the GR output is ~0.1 °C–~0.15 °C warmer than our reconstructions, and during the latter period, it is ~0.1 °C–~0.15 °C cooler. Discrepancies between our reconstructions and the GR output may indicate uncertainties in the external forcings in the GR model (Zorita et al., 2004). The TraCE-21ka GCM simulation (TraCE) from the LGM to the present (Liu et al., 2009; He, 2011; He et al., 2013), forced during the last millennium with greenhouse gas changes and only Milankovitch forcing on insolation (correspondence with Dr. Feng He), does not illustrate a LIA signal in the global or northern hemisphere surface temperatures or southern hemisphere tropical SSTs (Fig. 5a). Neither GCM captures precipitation rate variability similar to that in the summit accumulation record (Fig. 5b),

suggesting that these GCMs are unable to capture QIC precipitation rate variability. Proxy reconstructions of SSTs for the NINO4 region (5°N to 5°S; 160°E to 150°W) from the QIC ice core record of $\delta^{18}O$ (Thompson et al., 2013) find mild cooling during the later LIA period (readvance in the Qori Kalis valley (1660–1710 CE)) but no real trend during the earlier period (maximum glacier extent in the Qori Kalis valley (1490 CE ± 60 years)) (Fig. 5a). However, tropical SST reconstructions from Andes ice core $\delta^{18}O$ records differ in magnitude and trend (e.g. Thompson et al., 1995, 1998; Pierrehumbert, 1999; Thompson et al., 2013).

We constrain southern hemisphere tropical SSTs cooling during the YD to between 0.52 °C and 0.87 °C, with the lower bound corresponding to a 40% increase in precipitation and the upper corresponding to a precipitation scaling with Clausius–Clapeyron. For the situation where the glacier dynamics fundamentally changes, an upper extreme on SST coolings is ~1.4 °C at which point the freezing level height at the QIC would drop below the plateau base and the glacier would grow almost limitlessly. For a ~20% increase in the precipitation rate, which agrees with the trend in the TraCE simulation (Liu et al., 2009; He, 2011; He et al., 2013), we find a cooling of between 0.63 °C and 0.68 °C. The TraCE simulation (Liu et al., 2009; He, 2011; He et al., 2013), forced with changes in sea ice extent, continental configurations, meltwater fluxes, and Milankovitch forcing on insolation, suggest that the early YD (12.8–12.4 ka) tropical southern hemisphere climate was both cooler (~0.84 °C) and wetter (~20%) than present (Fig. 6) but that there is a ~0.2 °C SST warming trend and a ~10% precipitation rate increase going from the late Antarctic Cold Reversal (ACR) (13.5–12.8 ka) to the early YD. The TraCE temperature anomalies agree with our results in the limit where the precipitation rate scales with Clausius–Clapeyron. However, for a ~20% increase in the precipitation rate, our reconstructed SST cooling is ~0.2 °C less than the TraCE simulations. The upper extreme on cooling (freezing level height limit) greatly overestimates the SST coolings realized in the GCM. The proxy record from tropical marine cores in similar regions is conflicting. The Lea et al. (2003) reconstruction for the Cariaco Basin core (10.7°N; 64.9°W) finds significant SST cooling (3 °C–4 °C) from the late ACR to the YD while the Hüls and Zahn (2000) core for the Tobago Basin core (12.1°N; 61.2°W) finds mild warming from the ACR to the YD. Wan et al. (2009) illustrate how marine sediment core records capture local trends, which can differ from regional trends due to changes in sea level, ocean circulation, and upwelling.

Our paleoclimate reconstructions agree with GCM simulations that include forcing mechanisms that are believed to have been important in producing the century-scale and abrupt climate change events. Our LIA reconstruction finds a southern hemisphere SST cooling that agrees with the GR simulation (González-Rouco et al., 2006), which includes short-term insolation and volcanic aerosol forcings. However, our reconstruction and the GR simulation disagree with the TraCE simulation (Liu et al., 2009; He, 2011; He et al., 2013) for the last millennium, which does not include these forcings and does not illustrate a LIA trend. This disagreement and the lack of a LIA signature in the TraCE simulation possibly highlight the importance of short-term insolation and volcanic aerosol forcings in producing the temperature trends of the last millennium. Our YD reconstructions and TraCE simulation (Liu et al., 2009; He, 2011; He et al., 2013), which include many of the hypothesized late Pleistocene forcing mechanisms, indicate that the southern hemisphere tropics during the YD were both colder and wetter than present and agree on the whole. Despite the lack of a southern hemisphere tropical SST cooling trend from the late ACR into the early YD in the TraCE simulation, the bedrock slope profile of the Huancané valley is such that if the terminus were near the plateau base, a slight temperature or precipitation rate forcing would result in a significant readvance of the glacier. Following this YD readvance, the gradual SST warming into the Holocene realized in the TraCE simulation would quickly overpower any mass imbalance that might have caused the readvance to the Hu-II moraines, and the glacier would retreat. The geologic record suggests that the glacier retreated from the Hu-II moraine position to almost the Hu-I moraine position between ~12.35 ka and 11.6 ka (Kelly et al., 2012, 2015) and the climate trend in the TraCE simulation and the model work conducted here are consistent with this glacier length trend.

5. Conclusions

We conduct numerical simulations on the Huancané outlet glacier of the QIC to quantify the glacier length response to climate change and climate noise within an unchanging mean climate state. We also use the model to reconstruct possible paleoclimates, both at the ice cap and regionally, for the LIA and the YD. Our key results are the following:

- Over the range of plausible changes in air temperature and precipitation rate changes, air temperature changes are the dominant climate forcing mechanism for glacier length changes. The glacier advance for a 1 °C cooling is about one to four times the value of the glacier advance for a doubling in the precipitation rate. Also, the maximum observed decadal-averaged accumulation rate increase from the ice core record (Thompson et al., 2013) could produce less than half of the glacier advance necessary to reach the LIA moraines, in the absence of air temperature cooling.
- Glacier length fluctuations due to interannual climate variability are significantly smaller than the glacier advances necessary to form the Huancané valley moraines. Glacial features within ~400 m of the current ice margin may have been produced by glacier fluctuations due to contemporary interannual climate variability, but glacier advances more than twice as great as that are needed to form the geomorphic record.
- The observed geomorphic features in the Huancané valley can only be explained by a change in the mean climate state and require some degree of cooling.
- During the LIA, we reconstruct air temperature coolings at the ice cap of between ~0.7 °C and ~1.1 °C, corresponding to regional SST coolings of between ~0.4 °C and ~0.6 °C.
- During the YD, we reconstruct an upper bound on air temperature coolings at the ice cap of ~2.6 °C and a lower bound of ~0.9 °C, corresponding to regional SST coolings of between ~1.4 °C and ~0.5 °C.
- Our LIA and YD paleo-SST reconstructions from the geomorphic record of the Huancané outlet glacier of the QIC agree in magnitude and trend with GCM simulations that include forcing mechanisms that are believed to have caused the LIA and YD climate change events.

Acknowledgments

This work was supported by National Science Foundation grant EAR-1003686, EAR-1003460, and EAR-1003072. We thank Dr. Doug Hardy for access to the QIC meteorological station data for our model calibration, Dr. Eduardo Zorita for access to GR simulations of the last millenium, and Dr. Feng He for correspondence about the TraCE simulations. We thank Lonnie Thompson and our anonymous reviewer for constructive comments and feedback.

References

Anderson, B., Mackintosh, A., 2006. Temperature change is the major driver of late-glacial and holocene glacier fluctuations in New Zealand. Geology 34, 212–124.

Anderson, L.S., Roe, G.H., Anderson, R.S., 2014. The effects of interannual climate variability on the moraine record. Geology 42, 55–58.

Audebaud, E., 1973. Geología de los cuadrángulos de Ocongate y Sicuani. Serv. Geol. Min. Bol. 25, 72.

Baker, P.A., Seltzer, G.O., Fritz, S.C., Dunbar, R.B., Grove, M.J., Tapia, P.M., Cross, S.L., Rowe, H.D., Broda, J.P., 2001. The history of South American tropical precipitation for the past 25,000 years. Science 291, 640–643.

Bookhagen, B., Strecker, M.R., 2008. Orographic barriers, high-resolution TRMM rainfall, and relief variations along the eastern Andes. Geophys. Res. Lett. 35, L06403.

Braithwaite, R.J., Zhang, Y., 2000. Sensitivity of mass balance of five Swiss glaciers to temperature change assessed by turning a degree-day -model. J. Glaciol. 46, 7–14.

Bradley, R.S., Vuille, M., Diaz, H.F., Vergara, W., 2006. Threats to water supplies in the tropical Andes. Science 312, 1755–1756.

Bradley, R.S., Keimig, F.T., Diaz, H.F., Hardy, D.R., 2009. Recent changes in freezing level heights in the tropics with implications for deglaciation of high mountain regions. Geophys. Res. Lett. 36, L17701.

Chavez, V.A., Salas, A.G., Gutierrez, S.E., Cuadros, P.J., 1997. Geologia de los cuadrangulos de Corani y Ayapata; hojas 28-u y 28-v. Instituto Geologico Minero y Metalurgico.

Chiang, J.C.H., Bitz, C.M., 2005. Influence of high latitude ice cover on the marine intertropical convergence zone. Clim. Change 59, 32–52.

Doughty, A.M., Anderson, B.M., Mackintosh, A.N., Kaplan, M.R., Vandergoes, M.J., Barrell, D.J.A., Denton, G.H., Scaefer, J.M., Chinn, T.J.H., Putnam, A.E., 2013. Evaluation of lateglacial temperatures in the Southern Alps of New Zealand based on glacier modeling at Irishman Stream, Ben Ohau Range. Quat. Sci. Rev. 72, 160–169.

Fujita, K., 2008a. Influence of precipitation seasonality on glacier mass balance and its sensitivity to climate change. Ann. Glaciol. 48, 88–92.

Fujita, K., 2008b. Effect of precipitation seasonality on climate sensitivity of glacier mass balance. Earth Planet. Sci. Lett. 276, 14–19.

González-Rouco, J.F., Beltrami, H., Zorita, E., von Storch, H., 2006. Simulation and inversion of borehole temperature profiles in surrogate climates: spatial distribution and surface coupling. Geophys. Res. Lett. 33, L01703.

Goodman, A.Y., Rodbell, D.T., Seltzer, G.O., Mark, B.G., 2001. Subdivision of glacial deposits in southeastern Peru based on pedogenic development and radiometric ages. Quat. Res. 56, 31–50.

Harris, I., Jones, P.D., Osborn, T.J., Lister, D.,H., 2014. Updated high-resolution grids of monthly climatic observations – the CRU TS3.10 Dataset. Int. J. Climatol. 34, 623–642.

He, F., 2011. Simulation Transient Climate Evolution of the Last Deglaciation with CCSM3. Ph. D. dissertation. University of Wisconsin at Madison.

He, F., Shakun, J.D., Clark, P.U., Carlson, A.E., Liu, Z., Otto-Blisner, B.L., Kutzbach, J.E., 2013. Northern hemisphere forcing on southern hemisphere climate during the last deglaciation. Nature 494, 81–85.

Hock, R., 2005. Glacier melt: a review of processing and their modeling. Prog. Phys. Geogr. 29, 362–391.

Huber, U.M., Bugmann, H.K., Reasoner, M.A., 2005. Global Changes and Mountain Regions: an Overview of Current Knowledge. Springer, The Netherlands.

Hüls, M., Zahn, R., 2000. Millennial-scale sea surface temperature variability in the western tropical North Atlantic from planktonic foraminiferal census counts. Paleocenography 15, 659–678.

Huybers, K., Roe, G.H., 2009. Spatial patterns of glaciers in response to spatial patterns in regional climate. J. Clim. 22, 4606–4620.

Jomelli, V., Favier, V., Rabatel, A., Brunstein, D., Hoffmann, G., Francou, B., 2009. Fluctuations of glaciers in the tropical Andes over the last millennium and palaeoclimate implications: a review. Palaeogr. Palaeoclimatol. Palaeoecol. 281, 269–282.

Jomelli, V., Khodri, M., Favier, V., Brunstein, D., Ledru, M.P., Wagnon, P., Blard, P.H., Sicart, J.E., Braucher, R., Grancher, D., Bourls, D.L., Braconnot, P., Vuille, M., 2011. Irregular tropical glacier retreat over the Holocene epoch driven by progressive warming. Nature 474, 196–199.

Jomelli, V., Favier, V., Vuille, M., Braucher, R., Martin, L., Blard, P.H., Colose, C., Brunstein, D., He, F., Khodri, M., Bourls, D.L., Leanni, L., Riterknecht, V., Grancher, D., Francou, B., Ceballos, J.L., Fonseca, H., Liu, Z., Otto-Blisner, B.L., 2014. A major advance of tropical Andean glaciers during the Antarctic Cold Reversal. Nature 513, 224–228.

Kaser, G., 1995. Some notes on the behaviour of tropical glaciers. Bull. Inst. Fr. Études Andin. 24, 671–681.

Kaser, G., Hardy, D.R., Mölg, T., Bradley, R.S., Hyera, T.M., 2004. Modern glacier retreat on Kilimanjaro as evidence of climate change: observations and facts. Int. J. Climatol. 24, 329–339.

Kelly, M.A., Lowell, T.V., Applegate, P.J., Smith, C.A., Phillips, F.M., Hudson, A.M., 2012. Late glacial fluctuations of Quelccaya Ice Cap, southeastern Peru. Geology 40, 991–994.

Kelly, M.A., Lowell, T.V., Applegate, P.J., Phillips, F.M., Schaefer, J.M., Smith, C.A., Kim, H., Leonard, K., Hudson, A.M., 2015. A locally calibrated, late glacial ^{10}Be production rate from a low-latitude, high-altitude site in the Peruvian Andes. Quat. Geochronol. 26, 70–85.

Lea, D.W., Pak, D.K., Peterson, L.C., Hughen, K.A., 2003. Synchroneity of tropical and high-latitude Atlantic temperatures over the last glacial termination. Science 301, 1361–1364.

Laclercq, P.W., Oerlemans, J., 2012. Global and hemispheric temperature reconstructions from glacier length fluctuations. Clim. Dyn. 38, 1065–1079.

Licciardi, J.M., Schaefer, J.M., Taggart, J.R., Lund, D.C., 2009. Holocene glacier fluctuations in the Peruvian Andes indicate northern climate linkages. Science 325, 1677–1679.

Liu, Z., Otto-Bliesner, B.L., He, F., Brady, E.C., Tomas, R., Clark, P.U., Carlson, A.E., Lynch-Stieglitz, J., Curry, W., Brook, E., Erickson, D., Jacob, R., Kutzbach, J., Cheng, J., 2009. Transient simulation of last deglaciation with a new mechanism of Bølling-Allerød warming. Science 325, 310–314.

Mann, M.E., Zhang, Z., Rutherford, S., Bradley, R.S., Hughes, M.K., Shindell, D., Ammann, C., Faluvegi, G., Ni, F., 2009. Global signatures and dynamical origins of the Little Ice Age and medieval climate anomaly. Science 326, 1256–1260.

Mark, B.G., Seltzer, G.O., Rodbell, D.T., Goodman, A.Y., 2002. Rates of deglaciation during the last glaciation and Holocene in the Cordillera Vilcanota-Quelccaya Ice Cap region, southeastern Peru. Quat. Res. 57, 287–298.

Mercer, J.H., Thompson, L.G., Marangunic, C., Ricker, J., 1975. Peru's Quelccaya Ice Cap: glaciological and glacial geological studies, 1974. Antarct. J. U. S. 10, 19–24.

Mercer, J.H., Palacios, O.M., 1977. Radiocarbon dating of the last glaciation in Peru. Geology 5, 600–604.

Oerlemans, J., 1986. An attempt to simulate historic front variations of Nigardsbreen, Norway. Theor. Appl. Climatol. 37, 126–135.

Oerlemans, J., Fortuin, J.P.F., 1992. Sensitivity of glaciers and small ice caps to greenhouse warming. Science 258, 115–117.

Oerlemans, J., 1997a. Climate sensitivity of the Franz Josef Glacier, New Zealand, as revealed by numerical modeling. Arct. Alp. Res. 29, 233–239.

Oerlemans, J., 1997b. A flowline model for Nigardsbreen, Norway: projection of future glacier length based on dynamic calibration with the historic record. J. Glaciol. 24, 382–389.

Oerlemans, J., 2000. Holocene glacier fluctuations: is this current rate of retreat exceptional? Ann. Glaciol. 21, 2000.

Oerlemans, J., 2001. Glaciers and Climate Change. AA. Balkeman Publishers, Lisse.

Oerlemans, J., 2005. Extracting a climate signal from 169 glacier records. Science 308, 675–677.

Pepin, N., Bradley, R.S., Diaz, H.F., Baraer, M., Caceres, E.B., Forsythe, N., Fowler, H., Greenword, G., Hashmi, M.Z., Liu, X.D., Miller, J.D., Ning, L., Ohmura, A., Palazzi, E., Rangwala, I., Schoner, W., Severskiy, I., Shahgedoanova, M., Wang, M.B., Williamson, S.N., Yang, D.Q., 2015. Elevation-dependent warming in mountain regions of the world. Nat. Clim. Change 5, 424–430.

Pierrehumbert, R.T., 1995. Thermostats, radiator fins, and the local runway greenhouse. J. Atmos. Sci. 52, 1784–1806.

Pierrehumbert, R.T., 1999. Huascaran δ^{18}O as an indicator of tropical climate during the Last Glacial Maximum. Geophys. Res. Lett. 26, 1234–1248.

Pierrehumbert, R.T., 2011. Principles of Planetary Climate. Cambridge University Press, New York.

Placzek, C., Quade, J., Patchett, P.J., 2006. Geochronology and stratigraphy of late Pleistocene lake cycles on the southern Bolivian Altiplano: implications for causes of tropical climate change. Geol. Soc. Am. Bull. 118, 515–532.

Ramirez, E., Hoffmann, G., Taupin, J.D., Francou, B., Ribstein, P., Caillon, N., Ferron, F.A., Landais, A., Petit, J.R., Pouyaud, B., Schotterer, U., Simoes, J.C., Stievenard, M., 2003. A new Andean deep ice core from Navado Illimani (6350 m), Bolivia. Earth Planet. Sci. Lett. 212, 337–350.

Rind, D., Peteet, D., 1985. Terrestrial conditions at the Last Glacial Maximum and CLIMAP sea-surface temperature estimates: are they consistent? Quat. Res. 24, 1–22.

Roe, G.H., O'Neal, M.A., 2009. The response of glaciers to intrinsic climate variability: observations and models of late-Holocene variations in the pacific northwest. J. Glaciol. 55, 839–854.

Roe, G.H., 2011. What do glaciers tell us about climate variability and climate change? J. Glaciol. 57, 567–578.

Roe, G.H., Baker, M.B., 2014. Glacier response to climate perturbations: an accurate linear geometric model. J. Glaciol. 60, 670–684.

Sagredo, E.A., Rupper, S., VLowell, T., 2014. Sensitivity of the equilibrium line altitude to temperature and precipitation changes along the Andes. Quat. Res. 81 (2), 355–366.

Seager, R., Battisti, D.S., 2007. Challenges to Our Understanding of the General Circulation: Abrupt Climate Change in the Global Circulation of the Atmosphere. Princeton University Press, New Jersey, USA.

Seidel, D.J., Free, M., 2003. Comparison of lower-tropospheric temperature climatologies and trends at low and high elevation radiosonde sites. Clim. Change 59, 35–74.

Sobel, A.H., Nilsson, J., Polvani, L.M., 2001. The weak temperature gradient approximation and balanced tropical moisture waves. J. Atmos. Sci. 58, 3650–3665.

Stroup, J.S., Kelly, M.A., Lowell, T.V., Applegate, P.J., Howley, J.A., 2014. Late holocene fluctuations of the Qori Kalis outlet glacier, Quelccaya Ice Cap, Peruvian Andes. Geology. http://dx.doi.org/10.1130/G35245.1.

Taylor, R.G., Mileham, L., Tindimugaya, C., Majugu, A., Muwanga, A., Nakileza, B., 2006. Recent glacial recession in the Rwenzori Mountains of East Africa due to rising air temperature. Geophys. Res. Lett. 33, L10402.

Thompson, L.G., 1979. Glaciology of the Peruvian Quelccaya ice cap. Bol. Soc. Geol. Peru 63, 149–158.

Thompson, L.G., Mosley-Thompson, E., Bolzan, J.F., Koci, B.R., 1985. A 1500 year

record of climate variability recorded in ice course from the tropical Quelccaya Ice Cap. Science 229, 971–973.
Thompson, L.G., Mosley-Thompson, Dansgaard, W., Grootes, P.M., 1986. The "Little Ice Cage" as recorded in the stratigraphy of the tropical Quelccaya Ice Cap. Science 234, 361–364.
Thompson, L.G., Mosley-Thompson, E., Davis, M.E., Lin, P.N., Henderson, K.A., Cole-Dai, J., Bolzan, J.F., Liu, K.B., 1995. Late Glacial Stage and Holocene tropical ice core records from Huascaran, Peru. Science 269, 46–50.
Thompson, L.G., Davis, M.E., Mosley-Thompson, E., Sowers, T.A., Henderson, K.A., Zagorodnov, V.S., Lin, P.N., Mikhalenko, V.N., Campen, R.K., Bolzan, J.F., Cole-Dai, J., Francou, B., 1998. A 25,000-year tropical climate history from Bolivian ice cores. Science 282, 1858–1864.
Thompson, L.G., Mosley-Thompson, E., Brecher, H., Davis, M., Len, B., Les, D., Lin, Ping-Nan, Mashiotta, T., Mountain, K., 2006. Abrupt tropical climate change: past and present. Proc. Natl. Acad. Sci. 103, 10536–10543.
Thompson, L.G., Mosley-Thompson, E., Davis, M.E., Zagorondnov, V.S., Howat, I.M., Mikhalenko, V.N., Lin, P.N., 2013. Annually resolved ice core records of tropical climate variability over the past ~1800 years. Science 340, 945–950.
Vacco, D.A., Alley, R.B., Pollard, D., 2009. Modeling dependency of moraine deposition on climate history: the effects of seasonality. Quat. Sci. Rev. 28, 639–646.
Vuille, M., Francou, B., Wagnon, P., Juen, I., Kaser, G., Mark, B.G., 2008. Climate change and tropical Andean glaciers: past, present, and future. Earth-Sci. Rev. 89, 79–96.
Waelbroeck, C., Paul, A., Kucera, M., Rosell-Melé, A., Schneider, R., Mix, A.C., Abelmann, A., Armand, L., Bard, E., Barker, S., Barrows, T.T., Benway, H., Cacho, I., Chen, M.-T., Cortijo, E., Crosta, X., de Vernal, A., Dokken, T., Duprat, J., Elderfield, H., Eynaud, F., Gersonde, R., Hayes, A., Henry, M., Hillaire-Marcel, C., Huang, C.-C., Jansen, E., Juggins, S., Kallel, N., Kiefer, T., Kienast, M., Labeyrie, L., Leclaire, H., Londiex, L., Mangin, S., Matthiessen, J., Marret, F., Meland, M., Morey, A.E., Mulitza, S., Pflaumann, U., Pisias, N.G., Radi, T., Rochon, A., Rohling, E.J., Sbaffi, L., Schäfer-Neth, C., Solignac, S., Spero, H., Tachikawa, K., Turon, L.-J., 2009. Constraints on the magnitude and patterns of ocean cooling at the Last Glacial Maximum. Nat. Geosci. 2, 127–132.
Wan, X., Chang, P., Saravanan, R., Zhang, R., Schmidt, M., 2009. On the interpretation of Caribbean paleo-temperature reconstructions during the Younger Dryas. Geophys. Res. Lett. 36, L02701.
Williams, I.N., Pierrehumbert, R.T., Huber, M., 2009. Global warming, convective threshold, and false thermostats. Geophys. Res. Lett. 36, L21805.
Xu, K.M., Emanuel, K.A., 1989. Is the tropical atmosphere conditionally unstable? Mon. Weather Rev. 1187, 1471–1479.
Zorita, E., von Storch, H., González-Rouco, F., Cubasch, U., Luterbacher, J., Legutke, S., Fischer-Bruns, L., Schles, U., 2004. Climate evolution of the last five centuries simulated by an atmosphere - ocean model: global temperature, the North Atlantic Oscillation and the Late Maunder Minimum. Meteorol. Z. 13, 271–289.